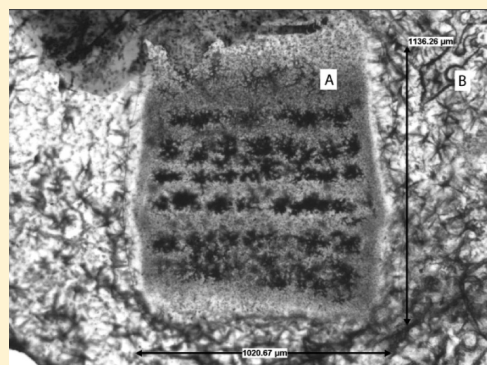


Effects of X-rays on Crystal Nucleation in Lithium Disilicate

Vladimir Martis,^{†,‡} Sergey Nikitenko,[†] Sabyasachi Sen,[§] Gopinathan Sankar,[‡] Wouter van Beek,^{||,¶} Yaroslav Filinchuk,^{||,∇} Irina Snigireva,[⊥] and Wim Bras^{*,†}[†]Netherlands Organization for Scientific Research (NWO), DUBBLE@ESRF, 6, Rue Jules Horowitz, 38000 Grenoble, France[‡]Department of Chemistry, University College London, Gordon Street, London WC1H 0AJ, United Kingdom[§]Department of Chemical Engineering and Materials Science, University of California Davis, Davis, California 95616, United States^{||}Swiss-Norwegian Beamlines at ESRF, 6, rue Jules Horowitz, 38000 Grenoble, France[⊥]European Synchrotron Radiation Facility, 6, rue Jules Horowitz, 38000 Grenoble, France^{*}Dipartimento di Scienze e Tecnologie Avanzate and Nano-SiSTeMI Interdisciplinary Centre, Università del Piemonte Orientale "A. Avogadro", Viale T. Michel 11, I-15121 Alessandria, Italy

ABSTRACT: The effects of exposure to a monochromatic 10 keV X-ray beam on thermally induced crystallization of lithium disilicate glass have been investigated and rendered two unexpected findings. First, it was found that an extended exposure during the nucleation heat treatment increased the number of nucleation sites. Second, it was observed that the effects extended far beyond the sample region that was directly exposed to the X-ray beam. The effects were confined to the direction perpendicular to the polarization of the synchrotron radiation beam that was used. The effects could be attributed to photo electrons created not only by the direct X-ray beam but also by the scattered radiation. Further evidence of the influence of photo electrons due to scattered X-rays is found in the results of an online crystallization study on a lysozyme solution.



INTRODUCTION

The use of synchrotron radiation-based X-ray techniques to follow the evolution of materials in time has become quite common in the past decade. The time domains available depend on which specific technique is used, but broadly speaking one can state that the most time-resolved experiments are performed at a rate of around 1–60 s/frame. Obviously, there are experiments where higher time resolution is required and also can be achieved, but these are not numerous. However, in many cases, it is not required or desirable to carry out experiments with too high a time resolution. Common sense tells us that when studying the drying of, for instance, cement, it is not too sensible to take data at a millisecond time frame rate. The same is true for many studies in catalysis or crystallization. Therefore, in many experiments, for example, hydrothermal synthesis of dense metal oxides catalysts at constant temperature or phase transformation during heating at elevated temperatures, is a sample exposed to the X-ray beam in an approximate energy range 5–20 keV for several minutes or hours.

In general, the danger of sample modification due to interactions with the X-ray beam is assumed to be relatively benign as compared to, for instance, electron microscopy. However, the danger for damage due to radiation by X-rays in this photon energy range is known but apart from in the protein crystallography community not very well documented.^{1,2} The key to combat the damage problem in organic crystals is to cool the

samples to cryogenic temperatures where the damage-causing processes are arrested. Unfortunately, the cooling strategy does not work when one wants to study time-resolved processes of samples where water is the solvent or where temperature is one of the controlling factors such as in crystallization processes.

In general, the influence of exposure to radiation with photons with energies 5–20 keV has a destructive tendency on either the molecules themselves or the crystals formed from these molecules. Monochromatic X-ray beams of third generation synchrotrons do not induce sufficient local heating effects to be the cause of this damage, and the effect has more to be sought in the radiolysis products liberated by X-ray absorption.³ However, in crystallization studies on polymers⁴ or in the solid state,⁵ the effects of the interaction of the X-rays with the sample have so far been ignored apart from microfocus experiments where the local dose is so high that not only the crystallization process is influenced but actually the sample can be destroyed.⁶

There are exceptions to the destructive effect of X-rays reported in the literature. In some cases, the X-ray beam actually caused particles to be formed,⁷ but these experiments were carried out with a pink beam, that is, partially monochromated and consequently a very high radiation dose and a possible case

Received: January 3, 2011

Revised: May 17, 2011

Published: May 18, 2011

for local heating. For experiments where monochromatic radiation was used, very few references of the interference of the X-rays with the crystallization process can be found. A report on radiation-induced crystallization of sucrose due to 8 keV photons from a sealed tube Cu source can be found.⁸ However, these authors worked on a system of “dried raspberry flavored Jell-O (gelatin)” in which the gelatin inhibited the formation of sucrose crystals. Once the sample was exposed to radiation for several hours, crystallization occurred. Although the authors do not provide an explanation for this phenomenon, it could well be that the radiation damaged the gelatin matrix sufficiently for the sucrose to become mobile and start crystallization. When exposed to microwave radiation (100 W, 2.4 GHz, 10–15 min exposures), the authors found a similar effect.

Several other cases have been reported in which radiation helped to induce structure formation. The initiation of pyramidally shaped crystals on the surface of 0.5 μm thick amorphous, mechanically buckled, barium titanate film when exposed to a dose of 10^{10} photons/s, 24 keV in a $12 \times 12 \mu\text{m}^2$ spot is to our knowledge the only example where radiation is assumed to induce surface crystallization on a solid sample.⁹ The authors dismiss the possibility that this might be due to local sample heating but instead make a reasonable case that the electrons created by the photoelectric effect increase the vibration amplitude in, mainly, the light atoms. Recently, an effect was reported in which the authors claimed to have found bundle formation under the influence of radiation.¹⁰ X-rays of around 8.5 keV are reported to have an effect on the glass transition temperature in polymethylmethacrylate (PMMA),¹¹ which could indicate an effect on the crystallization kinetics as well.

In this Article, we report some serendipitous findings of the interaction of 10 keV X-ray photons with a lithium disilicate (LiSi2) glass. The crystallization kinetics of this type of glass is widely studied through the years, and it is believed that crystallization is homogeneous throughout the bulk of the material.^{12–14} The idea of the experiment was to subject the sample to two-step heat treatment in which the first step would induce the crystallization nucleation centers and the second, higher temperature treatment, would allow the nucleation centers to develop into crystallites. By performing combined SAXS/WAXS experiments, one can gain insight into the growth of the particles and the crystalline volume fraction. In this way, the crystallization kinetics can be studied with, for instance, Avrami-type methods¹⁵ provided that the sample temperature is homogeneous and the newly formed crystallites are randomly oriented to avoid texture effects. In the case that texture due to surface crystallization exists, kinetic studies are more difficult because the texture degree might not remain the same during the experiment, and therefore one would observe peak intensity variations due to both growth as well as changing texture with little hope of being able to deconvolute the two effects.^{5,16}

There are commercial materials on the market, Fotoform and Fotoceram, which are based on LiSi2 that can be crystallized by exposure to ultraviolet radiation. However, a prerequisite for this behavior is that the glass is doped with both Ce as well as Ag.¹⁷ The mechanism involved is that upon irradiation the Ce releases electrons, which subsequently reduce the Ag to a metallic state. Upon raising the temperature, the Ag atoms become mobile and form metallic clusters, which in turn acts as the nucleus for the LiSi2 crystal to grow. In this work, we report on crystallization studies of pure LiSi2 without any dopant.

MATERIALS AND METHODS

LiSi2 ($\text{Li}_2\text{Si}_2\text{O}_5$) glass was prepared by batch melting (1 kg batch) of high-purity Li_2CO_3 and SiO_2 reagents in a Pt crucible at 1550 °C for 6 h. The melt was poured on graphite to form a 0.5 cm thick patty that was subsequently annealed at 450 °C for 30 min and cooled to room temperature by shutting off the furnace power. The patty was stored in a desiccator. Several plates of dimension 0.2×1.0 cm were cut from this patty using a Buehler diamond saw. Thin platelets (100 μm) were cut, and the surfaces were slightly polished using SiO_2 as polishing powder (SPL, Zaandam, Netherlands) to remove any inhomogeneity, which could act as surface nucleation centers. Because this material is slightly hygroscopic, care was taken to store the materials in a desiccator and to perform both the cutting as well as the polishing water free.

Fluorescence XAS measurements at the Pt L-edge and Au L-edge using a nine-element Ge detector were performed at DUBBLE (BM26A) at the European Synchrotron Radiation Facility (ESRF) to establish contamination levels due to materials from crucibles used for the sample preparation becoming incorporated into the sample. The concentration of Pt and Au in the sample was below the detectable level of the detector (<100 ppm), and therefore elemental contamination is assumed to be irrelevant for these studies.

SAXS/WAXS experiments were performed on BM26A at the ESRF¹⁸ and on beamline 7.3.3 at the Advanced Light Source (ALS, Berkeley).¹⁹ Both beamlines have comparable parameters. BM26A is designed as an EXAFS station but also has a SAXS/WAXS capability.¹⁸ The storage ring was operated in 7/8 + 1 filling mode with current between 160 and 200 mA at 6 GeV electron energy. Measurements were performed with monochromatic beam produced by Si(111) at energy of 10 keV. The acquisition time for frames was set to 60 s/frame. The full width beam spot on the sample was about $0.3 \times 1.0 \text{ mm}^2$ ($V \times H$), which was verified by measuring a beam mark on the green paper. In the vertical direction, there are no relevant intensity “tails”.²⁰ For a typical experiment, the average photon flux on the samples was 3.8×10^9 photons/s ($E = 10$ keV) from which around $(2.0 \pm 0.1) \times 10^9$ photons/s was absorbed in the sample. The absorbed energy, W_{abs} , will only marginally increase the sample temperature in the irradiated spot at room temperature.^{9,21} An upper limit of the temperature increase due to the X-ray absorption can be determined by assuming that there is no heat exchange between the irradiated volume and the surrounding matrix. The heat capacity and density of the material are, respectively, $C_p \approx 200 \text{ J/g} \cdot \text{K}$ and $\rho \approx 2.47 \times 10^{-3} \text{ g/mm}^3$. The irradiated volume is $V_{\text{irr}} \approx 0.05 \text{ mm}^3$. With the measured photon energy (10 keV), photon flux, and absorption, this leads to an adiabatic temperature rise (ATR) of $\text{ATR} = 1/\rho V_{\text{irr}} C_p \cdot W_{\text{abs}} \approx 1.4 \times 10^{-4} \text{ K/s}$. During 3 h nucleation heat treatment, the temperature will therefore rise at most 1.5 K.

The glass samples were mounted on the beamline in a “cage furnace” to avoid temperature gradients over the sample.²² In this furnace, the samples are positioned with a slight angle with respect to the direct beam. Therefore, the vertical beam footprint is about 25% larger than the actual vertical beam size. The temperature was measured by a Pt–Rh thermocouple placed close to the actual sample. The samples were subjected to a two-step heat treatment online, that is, the Tamman method.²³ The first nucleation induction step of 3 h was carried out at 450 ± 2 °C. The temperature was reached within 30 min at a rate of 15 °C/min. During this period, the samples absorbed a total radiation dose of 4.3×10^{13} photons/ mm^2 . No crystallization occurred during this initial thermal treatment. The second (crystallization) step was at a higher temperature ranging between experiments from 560 ± 2 to 650 ± 3 °C. The duration of the second step was determined by a combination of the temperature and the storage ring operation schedule: 10 h at 650 °C (fully crystallized, LidiSi-1); 5 h at 620 °C (not fully crystallized, LidiSi-2); 4 h at 600 °C (not fully crystallized, LidiSi-3); 10 h at 580 °C (LidiSi-4); and 12 h at 560 °C (LidiSi-5).

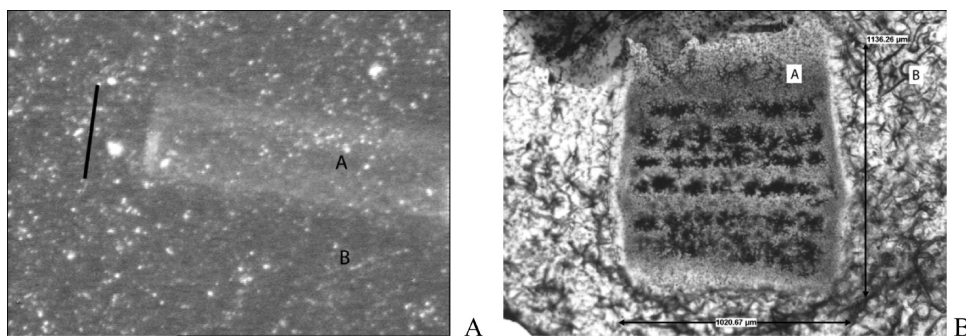


Figure 1. Optical microscopy from samples exposed to a $0.4 \times 4.0 \text{ mm}^2$ (panel A) and a $0.4 \times 1.0 \text{ mm}^2$ sized X-ray beam (panel B). Panel A (left-hand side) shows a not fully crystallized sample (heat treatment like sample LidiSi-3), and panel B (right-hand side) shows LidiSi-1 (fully crystallized). Only the central part of the areas marked “A” in both panels have been exposed to the beam during the crystallization experiment (vertical direction). The areas marked “B” have not been exposed to the direct beam. The black bar in panel A is $1 \pm 0.05 \text{ mm}$ in length.

The use of the combined SAXS/WAXS setup with the high temperature furnace does not guarantee a sufficiently accurate sample positioning with respect to the curved Inel detector. After being cooled, the samples were remeasured at room temperature on the Swiss-Norwegian beamline (BM1A) at the ESRF using a MAR345 image plate detector with a monochromatic beam ($\lambda = 0.7955 \text{ \AA}$). The sample–detector distance was 1968 mm. The X-ray beam size was set to $500 \times 500 \mu\text{m}$ ($V \times H$). With this beam size, it was possible to obtain diffraction data from both the areas exposed to X-rays during the online experiments as well as the nonexposed areas. Each pattern was collected during 5 s exposure. Analyses of diffraction data were carried out using FULL-PROF software.²⁴ The input parameters for the Rietveld refinement were based on the atomic coordinates determined from diffraction data for $\text{Li}_2\text{Si}_2\text{O}_5$ by de Jong.²⁵

Scanning electron microscopy (SEM) images were taken with a fully digital field-emission LEO Gemini 1530 (Carl Zeiss SMT) scanning electron microscope using an acceleration voltage of 20 keV. For the SEM sample preparation, the platelets were embedded in epoxy and subsequently cut with a diamond saw. The cross sections of the platelets were studied.

The online crystallization experiment of lysozyme sample preparation was carried out on a sample in which the capillary was held vertical in the X-ray beam. The detailed sample preparation is given elsewhere.²⁶ The online crystallization was initiated by salting out the sample by lowering the pH to 2.5 through the addition of 5N hydrochloric acid. Under normal conditions, that is, not while exposed to X-rays, this ensures a substantial amount of crystals to be formed within 10 min after the hydrochloric acid is added.

RESULTS

It should be remarked that no evidence for crystal formation was found in the samples during the initial nucleation heat treatment at $450 \text{ }^\circ\text{C}$. In all cases, crystallization only started when the samples were brought to the higher crystallization temperature.

When the samples were removed from the sample holder after the experiments, an obvious coloration showed where the sample was exposed to the X-ray beam. The samples had lost transparency and, depending on the exposure time, became “frosty white”. See Figure 1. This white area was in the vertical direction on either side around $200 \mu\text{m}$ larger than the footprint of the X-ray beam on the sample. In the vertical direction, the intensity in the beam “tails” is known to be negligible and does not extend beyond $10 \mu\text{m}$.²⁰ In the horizontal direction, there is hardly a discoloration beyond the area exposed to the beam. At the

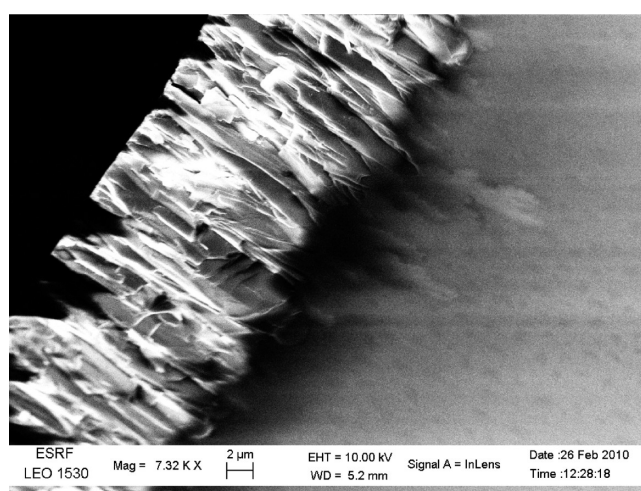


Figure 2. SEM micrograph of a freshly cleaved LidiSi-3, which has not been exposed to the X-ray beam. The black area is the epoxy in which the sample was embedded. A textured surface layer is observed. In the bulk, small fairly monodisperse droplets can be seen. These are assumed to be homogeneously nucleated bulk crystallites.

position where the X-ray beam has hit the sample, the affected area is around $15 \mu\text{m}$ larger than the actual X-ray footprint, which is consistent with the extent of the beam “tail” in this direction.

It is not uncommon that solid-state samples that have been kept at elevated temperatures on a synchrotron beam are discolored at the position where the sample intercepts the X-ray beam. Oxidation effects can possibly play a role here, and it is generally assumed that these are surface effects, while the bulk of the material is not altered. However, there is an unexpected finding here in that the affected area ($\sim 1000 \mu\text{m}$) is larger than the actual X-ray beam footprint on the sample ($\sim 400 \mu\text{m}$) in the vertical direction. This is the case for both the fully as well as the partially crystallized samples. In the horizontal direction, the discoloured region is commensurate with the beam footprint. This has been verified by repeating the experiment with different horizontal slit settings while subjecting the samples to a heat treatment like sample LidiSi-3.

To establish if there are any structural differences between the exposed and nonexposed parts of the samples, we first performed scanning electron microscopy (SEM) on a cross cut through a not exposed part of the LidiSi-3 sample. This sample should

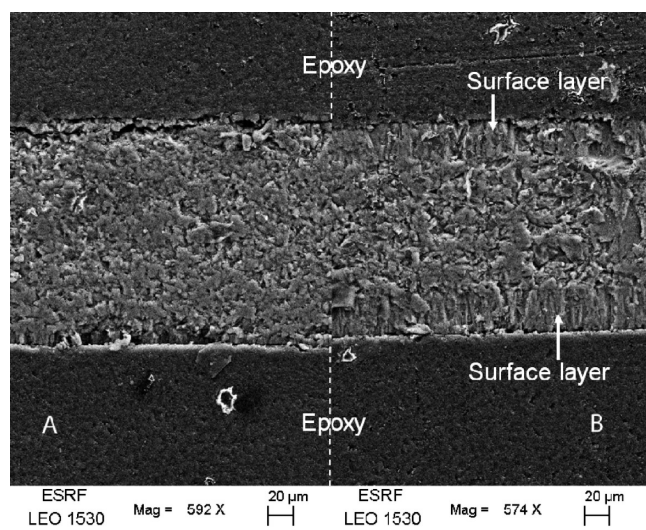


Figure 3. SEM micrographs of the cross section of an area exposed to X-rays during the online experiment (panel A) and a nonexposed area (panel B) for LidiSi-5 embedded in epoxy (dark regions, top and bottom of figure). The surface layers in the nonexposed sample are indicated by arrows. In the exposed area, there is hardly any evidence of a surface layer and the morphology is finer.

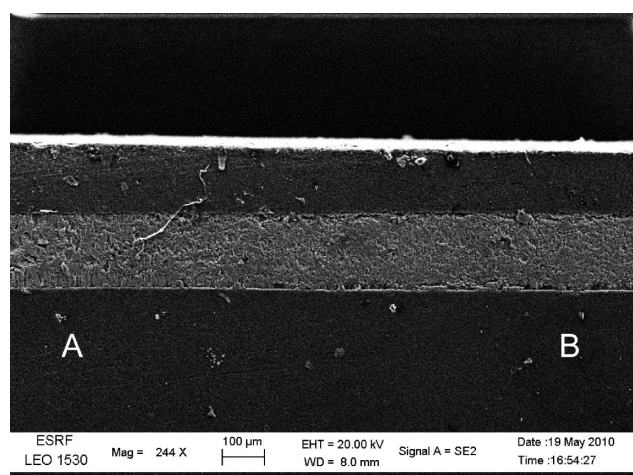


Figure 4. SEM micrograph of LidiSi-5 of the transition region between the nonexposed region (marked A) toward the exposed area (marked B). The nonexposed area clearly shows the surface layer and the coarse morphology, while in the exposed area the surface layer is absent and the morphology is finer.

according to the heat treatment be only partially crystallized. In this sample, we observe the presence of a textured surface layer; see Figure 2. LiSi₂ is a material that is supposed to exhibit bulk crystallization in preference over surface crystallization, but this finding is reproducible over several samples. The occurrence of the surface crystallization is not uncommon in this type of experiment. In the bulk of the not fully crystallized sample, small droplets of around 1 μm can be seen. On the basis of known bulk crystallization rates,²⁷ these are assumed to be small crystallites, although the required sample treatment to prove this by either X-ray or electron diffraction would be difficult and beyond the scope of this work.



Figure 5. The two-dimensional diffraction patterns from a not fully crystallized sample (LidiSi-2) for the area exposed to the X-rays during the experiment (panel A) and the nonexposed area (panel B). The irregular radial intensity in panel B is typical for coarse grained samples.

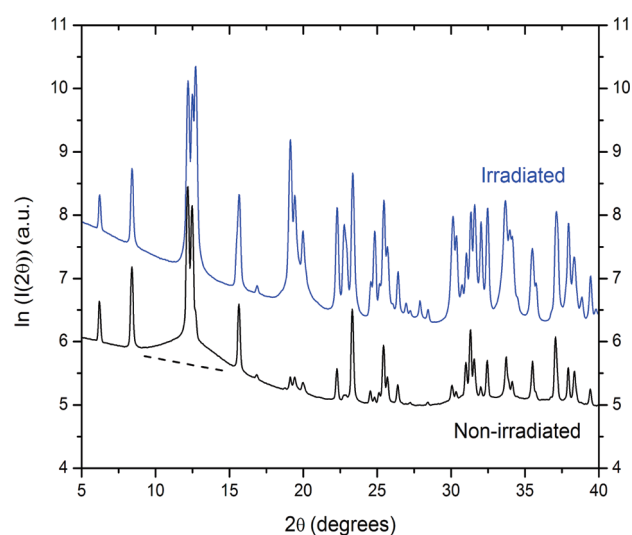


Figure 6. Powder diffraction data from the nonexposed area (black curve) we observe around $2\theta = 12^\circ$ scattering intensity, which is due to the amorphous halo (the dotted line is a guide to the eye). This intensity is absent in the curve taken in the exposed area (blue curve). The X-ray wavelength used was $\lambda = 0.7955 \text{ \AA}$.

When we compare the SEM micrographs of sample of the “exposed” with the “nonexposed” areas, there are two striking differences. “Exposed” in this context means “exposed to X-rays during both the nucleation as well as the crystallization heat treatment”. The surface layer that is observed in the nonexposed area is much reduced in size or even completely absent in the exposed area. The second difference is that the morphology in the nonexposed area is coarser as compared to the exposed area. The average crystallite size is estimated to be roughly twice as large. See Figure 3.

To eliminate any uncertainty, we have obtained a SEM micrograph for LidiSi-2 from the transition zone of the exposed to nonexposed area. This is shown in Figure 4. From this result, we can conclude that the influence of the X-rays is not limited to the surface but that the bulk of the material is also altered.

Powder diffraction patterns of all samples were obtained from both the exposed as well as the nonexposed sample areas. An example of patterns from LidiSi-2 that was not yet fully crystallized before the experiment was terminated is shown in Figure 5,

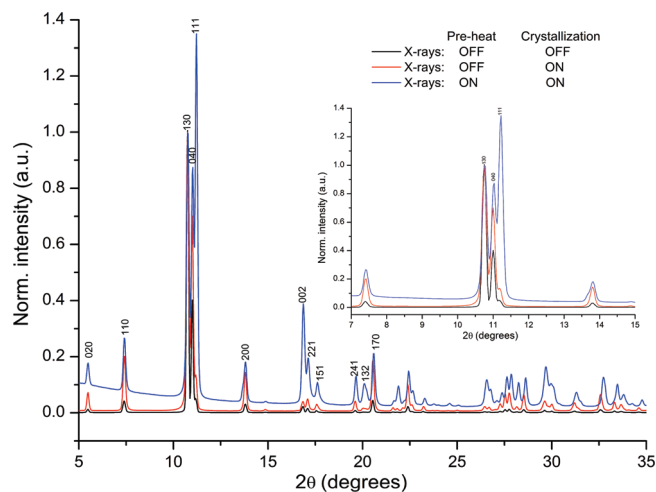


Figure 7. Powder diffraction data comparisons between samples areas exposed to X-rays at different stages of the thermal treatment. The peak intensities are normalized on the 130 diffraction peak. The inset shows a magnified range where we observe that the 040 and 111 peaks are weaker in the diffraction curves for the areas that were less or not exposed to X-rays during the experiment.

where panel “A” shows the diffraction pattern from a sample area that has been exposed to the X-ray beam and “B” corresponds to a nonexposed area.

In the area that was exposed to the X-rays during the experiment, one finds a regular powder pattern without the irregular intensity variations that occur in samples that consist of coarse grains in which too few grains have been exposed to the X-ray beam to generate a fully isotropic pattern. However, we find for the same sample in a region not exposed to the X-rays during the experiment a rather irregular radial intensity distribution, which is indicative of coarse crystals. In the nonexposed area, there is also an absence or severe intensity reduction in a number of diffraction peaks. This indicates the existence of crystallographic texture in the sample.

A radial integration will obviously not render accurate intensities in the case of the textured pattern. However, this can still be used for unit cell determinations. Because this sample was not fully crystallized, there is still scattering intensity remaining from the amorphous glass. In Figure 6, the result of a radial integration is shown.

In the diffraction pattern of the nonexposed area, remnants are found of the scattering halo due to the amorphous glass, which is consistent with the degree of crystallization that should have developed due to the thermal treatments. However, in the diffraction pattern obtained from the exposed area, this halo is absent. In fully crystallized samples, the amorphous halo is completely absent in both the exposed and the nonexposed areas. From these observations, we can draw the conclusion that inside the exposed area the crystallization progresses faster than outside the exposed area.

The powder diffraction unit cell characterization showed no difference between regions that that were grown while irradiating or in the absence of the beam but confirmed the presence of a single crystalline phase. Therefore, the surface layer crystallizes in the same phase as the bulk even though the morphology appears to be different. The room temperature parameters of this crystalline phase are orthorhombic, space group *Ccc2*, $a = 5.8299 \pm 0.0005$, $b = 14.6012 \pm 0.001$, $c = 4.7832 \pm 0.0005$.

Table 1. March Parameter G_1^{-2} and the Degree of the Texture η as a Function of the Exposure to X-rays during the Two-Step Thermal Treatment^a

X-rays		G_1^{-2}	η (%)
pre-heat	crystallization		
on	on	0.93 ± 0.02	4
off	on	1.13 ± 0.02	7
off	off	2.06 ± 0.07	40
on	off	not performed	

^a The columns “pre-heat” and “crystallization” indicate if the sample was exposed to the radiation during these thermal stages.

A further investigation was made on samples that were nonexposed, only exposed during the crystallization heat treatment, and a sample that was exposed during both the preheat as well as the crystallization treatment. The results of this are given in Figure 7 in which the respective diffraction curves are shown. In this figure, the peak intensities are normalized on the 130 diffraction peak. In the inset in the figure, a systematic intensity decrease can be seen in the 040 and 111 diffraction peaks. The curve related to the nonexposed area has the lowest intensity, while the pattern corresponding to an area that was irradiated during both the nucleation as well as the crystallization heat treatment has diffraction intensities, which compare well with the powder diffraction data that are found in the literature.²⁵

In Table 1, the results of the Rietveld refinement are shown as obtained with the software package Fullprof.²⁴ The March function²⁸ implemented in Fullprof is used to correct intensities for the preferred orientation in Debye–Scherrer geometry and renders that the March parameter G_1^{-2} value equal to 1 means perfect isotropic powder, <1 can in this case be related to the “platy” morphology, and >1 indicates the presence of texture. The degree of texture, η , can be determined from the March parameter.²⁹

The relevance here is not so much the actual degree of texture but the presence or absence of texture as a function of the exposure to the X-ray beam. We should not forget that the samples were platelets, but from these results it is clear that the samples that were exposed to the X-rays during both the preheat treatments as well as the crystallization treatment have a “platy” type of morphology, which is in agreement with earlier findings.³⁰ The samples that were only exposed during the crystallization have a somewhat textured morphology, and the samples that were not exposed to X-rays are rather heavily textured.

DISCUSSION

The morphology of LiS₂ glass that is subjected to a two-step heat treatment is found to be different as a function of exposures to X-rays during the different steps. In the case that the sample is not exposed, a surface layer and a bulk morphology with coarse crystallites is formed, which is heavily textured. If the same sample is exposed to the X-rays only during the crystallization step but not during the nucleation step, a lighter textured morphology is obtained. The most interesting phenomenon is found when the sample is exposed both during the nucleation as well as during the crystallization step. Next, an isotropic diffraction pattern is found with the earlier reported “platy” morphology.²⁵ There is also a marked difference in the amorphous glass content of samples that have been allowed to partially crystallize. The degree of crystallinity in the exposed areas of such

samples is higher than that in the nonexposed areas. Because of a lack of samples in the batch that we have used, we have not been able to study samples that were only exposed during the nucleation heat treatment.

From our data, it is clear that the X-rays influence the crystallization process. The fact that one finds a finer morphology and a faster crystallization rate when the sample is exposed during the nucleation heat treatment provides strong evidence to an increase in the number of crystallization nucleation sites that are being created in this step. What exactly the mechanism is by which this takes place is unclear. It has been reported that photoluminescence can be induced in LiS₂ after exposure to low energy X-rays, but,³¹ as far as we know, no influence on structure formation has been observed.

It has been found that in mechanically stressed amorphous BaTiO₃ films nonthermal crystallization occurred upon exposure to rather high doses of 24 keV X-rays.⁹ The authors explain this by an increase of the thermal vibration energy due to interactions with energetic photo electrons. This could increase the hopping probability, of especially the lighter atoms present in the sample. However, in the BaTiO₃ case, the effects were confined to the surface and to the area directly exposed to the X-rays. However, the recoil energy transmitted by the electrons is still rather low, and electronic excitations (photo excitation and subsequent Auger decay) might play a much more important role. Noteworthy, these processes are known to be the main contributor for X-ray-induced atom or ion desorption from surfaces.

Studies of crystalline materials with amorphous zones created by ion implantation irradiated by low energy electrons have shown that even far below the energy required to induce atomic displacements it is possible that recrystallization is induced. Interactions that create dangling bonds are sufficient and do not have to be supported by kinetic energy transfer from either the photons or the electrons to allow migration of atomic species.^{32,33} This is a plausible explanation for the phenomena that we observe with respect to the increased crystallization.

In the optical microscopy data, we find that the spot affected by the X-ray beam is substantially larger than the size of the beam itself. An area with the same horizontal size as the X-ray beam footprint but extending around 125 μm in the vertical direction on either side of the directly irradiated region is discolored and has the same fine morphology as the area directly exposed to the X-ray beam. We emphasize that no sizable extension is observed in the horizontal direction. The path length of both elastically as well as inelastically scattered electrons in the solid state is at most some micrometers and therefore not sufficient to explain the rather large extension in the vertical plane. A possible explanation can possibly be found in the fact that synchrotron radiation is polarized in the horizontal, that is, electron orbit, plane. Both elastically as well as inelastically scattered photons will scatter in the vertical direction. The scattered photons will have an energy distribution with a maximum of the original 10 keV photons energy and, assuming a density of 2.35 g/cm³ for the glass, an attenuation path length of around 275 μm in this sample. Photons that are initially inelastically scattered will have a shorter range. Photo electrons can be created anywhere in the volume throughout which the X-rays are scattered so that the nucleating effects do not have to remain confined to the direct exposed area of the sample.

The absence of a surface layer with a different texture but identical crystalline phase could also be explained in this scenario. Apparently surface nucleation is not completely irrelevant for our samples and has been observed by other authors as well.³⁴ If the

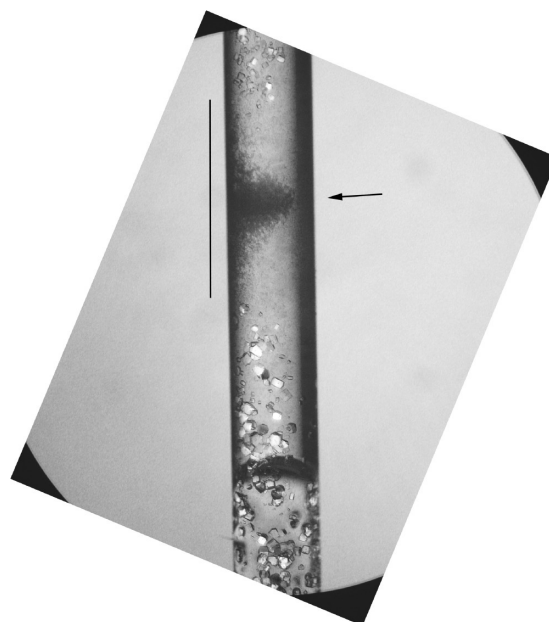


Figure 8. Online lysozyme crystallization experiment. The black dot indicated by the arrow indicates where the sample was exposed to the X-rays ($\sim 300 \mu\text{m}$). The diagonal bar indicates the length of the zone around the exposed spot where no crystallites could be found ($\sim 600\text{--}800 \mu\text{m}$ on either side of the beam spot). The capillary was positioned at right angles with respect to the polarization of the X-ray beam.

samples have been exposed to X-rays during the nucleation heat treatment, sufficient nucleation sites could have been formed throughout the sample and thus also near the surface, to ensure that the surface nucleation would become less important. A test of this hypothesis could be to expose a thick sample to the X-ray beam so that only a single surface of the sample platelet would receive sufficient flux.

In the Introduction, we mentioned that in most cases the influence of radiation had a destructive effect on crystalline structures. With the findings in this work that this was not limited to the area directly exposed to X-rays but could extend well beyond this region, we also have been able to explain a failure of an online crystallization experiment on lysozyme that possible could be attributed to radiolysis due to scattered X-rays. Figure 8 shows a capillary with a lysozyme solution in which crystallization was induced. The dark spot marked with an arrow marks where the capillary was exposed to a synchrotron beam of 300 μm in both the vertical as well as the horizontal direction. There is an “exclusion” of around 500 μm on either side where no crystallites can be found. Beyond this region, one finds crystallites that show the normal X-ray diffraction. Local heating effects can be ruled out again because even though the heat capacity of water, $C_{p,\text{water}} \approx 4.2 \text{ J/g}\cdot\text{K}$, is much lower as compared to the LiS₂ sample, the potential temperature increase would still be minimal.

Initially, we have assumed that the crystallization was inhibited by free radicals and possible other hydrolysis products generated by the interaction of the X-rays with the buffer solution. However, the combination of the lifetime of radiolysis products and the diffusion rates cannot explain the rather large distance over which no crystals are found.³ The maximum path length of any of the radiolysis products is less than 2 μm . The attenuation path length of X-ray photons in this example, however, is around

1.5 mm, and it is therefore plausible that the radiolysis products generated not only by the direct beam but also by the scattered X-ray photons are sufficient to inhibit crystallization.

CONCLUSION

The data that we have collected on Li₂S₂ samples provide strong evidence that an exposure to monochromatic synchrotron radiation even from a bending magnet source increases the crystallization nucleation rate if the sample is exposed to the radiation during the crystallization experiment. This is a rather unexpected finding because in general one finds the effects of high flux X-rays to be destructive instead of inducing crystallization.

The crystallization progresses faster in regions that have been exposed to X-rays. The two explanations that are feasible are that the crystal nucleation rate is higher or that the crystallization process itself is assisted by the X-rays. The latter option is rather unlikely, and the fact that we find a finer morphology in the samples where they have been exposed to X-rays favors the explanation that the nucleation sites are more abundant in the exposed area. What exactly the mechanism is that induces the nucleation is not clear at present, but local heating due to X-ray absorption and structural changes due to the kinetic energy of photoelectrons, created by absorption of the X-rays, can be ruled out. The most plausible explanation is that this is caused by the influence of the photo electrons on dangling bonds.

The experiments show that the effects due to radiation extend spatially well beyond the area directly exposed to X-rays in the direction at right angles to the X-ray beam polarization. The only explanation for the spatial extension of radiation effects beyond the directly exposed spot is that this is due to the absorption of X-rays that already have been scattered. The intensity of this scattered radiation is several orders of magnitude lower as compared to the direct beam, but when using a (medium intensity) beamline on a third generation synchrotron radiation source the number of scattered photons apparently is still numerous enough to interfere in a non negligible way with the samples in both the solid as well as the liquid state.

The original aim of the experiment was to study the crystallization kinetics of lithium disilicate samples when subjected to a two-step heat treatment by online SAXS/WAXS experiments. This two-step treatment was intended to separate the nucleation events from the crystallization growth and induce heterogeneous nucleation in the bulk of the material. Our results show that this approach for this particular glass can only be applied when care is taken to minimize the radiation dose and especially avoid the exposure to X-rays during the thermal treatment intended to induce crystallization nuclei.

AUTHOR INFORMATION

Corresponding Author

*Tel.: ++33-476882351. E-mail: wim.bras@esrf.eu.

Present Addresses

^YY. Filinchuk Institute of Condensed Matter and Nanosciences, Université Catholique de Louvain, Place L. Pasteur 1, B-1348 Louvain-la-Neuve, Belgium.

ACKNOWLEDGMENT

Our colleagues Jorg Zegenhagen (ESRF), Maarten Vos (ANU), Phil Pattison (SNBL), and Velimir Radmilovic (NCEM) are

thanked for discussions. The referees are acknowledged for their constructive remarks. The staff at beamlines 7.3.3 (ALS) and BM26 (ESRF) is gratefully acknowledged for their support.

REFERENCES

- (1) Nave, C.; Garman, E. F. Towards an understanding of radiation damage in cryocooled macromolecular crystals. *J. Synchrotron Radiat.* **2005**, *12*, 257–260.
- (2) Garman, E. F.; McSweeney, S. M. Progress in research into radiation damage in cryo-cooled macromolecular crystals. *J. Synchrotron Radiat.* **2007**, *14*, 1–3.
- (3) Roots, R.; Okada, S. Estimation of life times and diffusion distances of radicals involved in X-ray-induced DNA strand breaks or killing of mammalian-cells. *Radiat. Res.* **1975**, *64*, 306–320.
- (4) Fairclough, J. P. A.; Mai, S. M.; Matsen, M. W.; Bras, W.; Messe, L.; Turner, S. C.; Gleeson, A. J.; Booth, C.; Hamley, I. W.; Ryan, A. J. Crystallization in block copolymer melts: Small soft structures that template larger hard structures. *J. Chem. Phys.* **2001**, *114*, 5425–5431.
- (5) Bras, W.; Clark, S. M.; Greaves, G. N.; Kunz, M.; van Beek, W.; Radmilovic, V. Nanocrystal growth in cordierite glass ceramics studied with X-ray scattering. *Cryst. Growth Des.* **2009**, *9*, 1297–1305.
- (6) Davies, R. J.; Burghammer, M.; Riekel, C. Micro-Raman spectroscopy as an in situ tool for probing radiation damage during microdiffraction experiments in soft condensed matter. *Macromolecules* **2008**, *41*, 7251–7253.
- (7) Mesu, J. G.; van der Eerden, A. M. J.; de Groot, F. M. F.; Weckhuysen, B. M. Synchrotron radiation effects on catalytic systems as probed with a combined in-situ UV–vis/XAFS spectroscopic setup. *J. Phys. Chem. B* **2005**, *109*, 4042–4047.
- (8) Susich, G.; King, A. O.; Dogliotti, L. M. Radiation-induced crystallization of sucrose. *Science* **1959**, *130*, 567–568.
- (9) Feldman, Y.; Lyahovitskaya, V.; Leitus, G.; Lubomirsky, I.; Wachtel, E.; Bushuev, V. A.; Vaughan, G.; Barkay, Z.; Rosenberg, Y. X-ray initiation of nonthermal growth of single crystal pyramids in amorphous barium titanate. *Appl. Phys. Lett.* **2009**, *95*, 3.
- (10) Cui, H. G.; Pashuck, E. T.; Velichko, Y. S.; Weigand, S. J.; Cheetham, A. G.; Newcomb, C. J.; Stupp, S. I. Spontaneous and X-ray-triggered crystallization at long range in self-assembling filament networks. *Science* **2010**, *327*, 555–559.
- (11) Keymeulen, H. R.; Diaz, A.; Solak, H. H.; David, C.; Pfeiffer, F.; Patterson, B. D.; van der Veen, J. F.; Stoykovich, M. P.; Nealey, P. F. Measurement of the X-ray dose-dependent glass transition temperature of structured polymer films by X-ray diffraction. *J. Appl. Phys.* **2007**, *102*, 013528.
- (12) Greer, A. L.; Kelton, K. F. Nucleation in lithium disilicate glass - a test of classical-theory by quantitative modeling. *J. Am. Ceram. Soc.* **1991**, *74*, 1015–1022.
- (13) Fokin, V. M.; Zanutto, E. D.; Yuritsyn, N. S.; Schmelzer, J. W. P. Homogeneous crystal nucleation in silicate glasses: A 40 years perspective. *J. Non-Cryst. Solids* **2006**, *352*, 2681–2714.
- (14) James, P. F. Kinetics of crystal nucleation in lithium silicate glasses. *Phys. Chem. Glasses* **1974**, *15*, 95–105.
- (15) Bamford, H.; Tipper, C. In *Comprehensive Chemical Kinetics*; Bamford, H., Tipper, C., Eds.; Elsevier: New York, 1980; Vol. 22, Chapter 3.
- (16) Bras, W.; Greaves, G. N.; Oversluizen, M.; Clark, S. M.; Eeckhaut, G. The development of monodispersed alumino-chromate spinel nanoparticles in doped cordierite glass, studied by in situ X-ray small and wide angle scattering, and chromium X-ray spectroscopy. *J. Non-Cryst. Solids* **2005**, *351*, 2178–2193.
- (17) Veiko, V. P.; Kieu, Q. K.; Nikonorov, N. V.; Shur, V. Y.; Luches, A.; Rho, S. Laser-induced modification of glass-ceramics microstructure and applications. *Appl. Surf. Sci.* **2005**, *248*, 231–237.
- (18) Nikitenko, S.; Beale, A. M.; van der Eerden, A. M. J.; Jacques, S. D. M.; Leynaud, O.; O'Brien, M. G.; Detollenaere, D.; Kaptein, R.; Weckhuysen, B. M.; Bras, W. Implementation of a combined

SAXS/WAXS/QEXAFS set-up for time-resolved in situ experiments. *J. Synchrotron Radiat.* **2008**, *15*, 632–640.

(19) Hexemer, A.; Bras, W.; Glossinger, J.; Schaible, E.; Gann, E.; Kirian, R.; MacDowell, A.; Church, M.; Rude, B.; Padmore, H. A SAXS/WAXS/GISAXS beamline with multilayer monochromator. *J. Phys.: Conf. Ser.* **2010**, *247*, 012007.

(20) van Silfhout, R.; Kachatkou, A.; Kyele, N.; Scott, P.; Martin, T.; Nikitenko, S. High-resolution transparent x-ray beam location and imaging. *Opt. Lett.* **2011**, *36*, 570–572.

(21) Cheng, A. C.; Caffrey, M. Free radical mediated X-ray damage of model membranes. *Biophys. J.* **1996**, *70*, 2212–2222.

(22) Dent, A. J.; Oversluizen, M.; Greaves, G. N.; Roberts, M. A.; Sankar, G.; Catlow, C. R. A.; Thomas, J. M. A furnace design for use in combined X-Ray-absorption and diffraction up to a temperature of 1200 °C - Study of cordierite ceramic formation using fluorescence qexafs/xrd. *Physica B* **1995**, *209*, 253–255.

(23) Tammann, G. *Z. Phys. Chem.* **1898**, 441.

(24) Rodriguezcarvajal, J. Recent advances in magnetic-structure determination by neutron powder diffraction. *Physica B* **1993**, *192*, 55–69.

(25) De Jong, B.; Super, H. T. J.; Spek, A. L.; Veldman, N.; Nachtegaal, G.; Fischer, J. C. Mixed alkali systems: Structure and Si-29 MASNMR of Li₂Si₂O₅ and K₂Si₂O₅. *Acta Crystallogr., Sect. B: Struct. Sci.* **1998**, *54*, 568–577.

(26) Basso, S.; Fitch, A. N.; Fox, G. C.; Margiolaki, I.; Wright, J. P. High-throughput phase-diagram mapping via powder diffraction: a case study of HEWL versus pH. *Acta Crystallogr., Sect. D: Biol. Crystallogr.* **2005**, *61*, 1612–1625.

(27) Soares, P. C.; Zanotto, E. D.; Fokin, V. M.; Jain, H. TEM and XRD study of early crystallization of lithium disilicate glasses. *J. Non-Cryst. Solids* **2003**, *331*, 217–227.

(28) Dollase, W. Correction of intensities for preferred orientation in powder diffractometry: application of the March model. *J. Appl. Crystallogr.* **1986**, *19*, 267–272.

(29) Zolotoyabko, E. Determination of the degree of preferred orientation within the March-Dollase approach. *J. Appl. Crystallogr.* **2009**, *42*, 513–518.

(30) Tulyaganov, D. U.; Agathopoulos, S.; Kansal, I.; Valerio, P.; Ribeiro, M. J.; Ferreira, J. M. F. Synthesis and properties of lithium disilicate glass-ceramics in the system SiO₂-Al₂O₃-K₂O-Li₂O. *Ceram. Int.* **2009**, *35*, 3013–3019.

(31) Doi, A. Radiation-induced centers in lithium disilicate glass. *Jpn. J. Appl. Phys.* **1978**, *17*, 279–282.

(32) Jencic, I.; Bench, M. W.; Robertson, I. M.; Kirk, M. A. Electron-beam-induced crystallization of isolated amorphous regions in Si, Ge, GaP, and GaAs. *J. Appl. Phys.* **1995**, *78*, 974–982.

(33) Frantz, J.; Tarus, J.; Nordlund, K.; Keinonen, J. Mechanism of electron-irradiation-induced recrystallization in Si. *Phys. Rev. B* **2001**, *64*, 125313.

(34) Burgner, L. L.; Weinberg, M. C.; Lucas, P.; Soares, P. C.; Zanotto, E. D. XRD investigation of metastable phase formation in Li₂O-2SiO₂ glass. *J. Non-Cryst. Solids* **1999**, *255*, 264–268.